A COMPUTATIONAL DENSITY FUNCTIONAL THEORY INVESTIGATION OF THE INTERACTION OF BORON NITRIDE NANOSHEETS WITH MULTIPLE MOLECULAR HYDROGENS

Pek-Lan Toh[1a]*, Syed Amir Abbas Shah Naqvi[2a], Suh-Miin Wang[3a], Yao-Cong Lim[4a], Lee-Sin Ang[5b] and Lan-Ching[6c]

Abstract: In this study, the adsorption of molecular hydrogens (H_2) on boron nitride (BN) frameworks was investigated using the density functional theory (DFT) technique. The results of optimized geometric structures revealed that molecular hydrogens were favourably adsorbed on top of nitrogen atoms in the BN monolayers. In addition, the optimized equilibrium geometries were utilized to calculate the electronic structures, including binding energies, energies of the highest and lowest occupied molecular orbitals (HOMO and LUMO), molecular electrostatic potentials (MEPs), and Mulliken atomic charges (MACs). The binding energy values were calculated to be approximately 0.01 eV per molecular hydrogen based on the results. As the number of molecular hydrogens increased in the BN framework, a slight increase was observed in the binding energy value per hydrogen molecule. Furthermore, the HOMO–LUMO gaps were determined with the corresponding energy values of about 6 eV. Regarding the Frontier molecular orbitals (FMOs) diagrams, the electron densities for the HOMOs of the studied systems were primarily focused on the N-edges. Conversely, for the LUMO, the electron density distribution was localized in the B-edges of titled systems. In the context of hydrogen adsorption on BN nanosheets, the MEP maps indicated that hydrogen atoms at the N-edges of the studied systems exhibited the most positive electrostatic potentials in this research. In contrast, surfaces with negative electrostatic potential surfaces were situated in the region close to B-edges. The computed results are consistent with the corresponding Mulliken atomic charge distributions. From the analyses of the Mulliken scheme, all nitrogen atoms displayed negative charge values, and positive charges were found on the boron atoms. The DFT results obtained in this report may serve as the foundation for developing hydrogen storage materials..

Keywords: Density functional theory, boron nitride frameworks, hydrogen molecules, electronic structures

1. Introduction

Boron nitride (BN) is an inorganic compound composed of equal numbers of nitrogen (N) and boron (B) atoms (Mukasyan, 2017). According to literature studies, BN finds significant use in electronic and optoelectronic devices (Izyumskaya et al., 2017; Gonzalez–Ortiz, 2020). For instance, Izyumskaya et al. (2017) summarized an overview of the structural and physical properties of various polymorphs of BNs. Four crystal phase forms of BN exist cubic, hexagonal, wurtzite, and rhombohedral. Among these, hexagonal boron nitride (h-BN) stands out due to its wide bandgap energy, rendering it increasingly attractive for electronic and optoelectronic applications. Recent years have witnessed a growing interest in exploring the applications of BNs due to their unique chemical and physical structures, including excellent thermal shock resistance, low toxicity, favourable dielectric properties, high hydrogen storage capacity, and more (Izyumskaya et al., 2017; Gonzalez–Ortiz, 2020). In 2020, Gonzalez–Ortiz et al. discussed ongoing advancements in optimal synthesis methods and applications of BN-based materials. Their work presented four synthesis methods of BN-based nanostructured materials: in situ intercalative polymerization, melt-intercalation, solvent mixing, and template synthesis.

Numerous experimental studies have been conducted on BN nanomaterials (Kannan et al., 2013; Ansaloni & Sousa, 2013). For example, Kannan et al. (2013) employed a novel combustion synthesis method, glycine-nitrate, to synthesize h-BN crystals. For this purpose, they utilized Fourier transform infrared (FT-IR) spectroscopy and X-ray powder diffraction (XRD) to identify and characterize the h-BN compounds. Their experimental findings revealed the successful production of pure h-BN, which holds promise for high–temperature applications. Similarly, Ansaloni and Sousa, in the same year, synthesized and characterized the h-BN nanostructured sample. Their findings indicated that h-BN nanomaterial could be obtained through high–temperature treatment at 1600 °C. Notably, h-Bn nanostructures exhibit

Authors information:

[a]Faculty of Engineering and Green Technology, Universiti Tunku Abdul Rahman, 31900 Kampar, Perak, MALAYSIA. E-mail: tohpl@utar.edu.my[1]; syedamirnaqvi.51214@1utar.my[2]; wangsm456@1utar.my[3]; yaocong61@1utar.my[4]

[b]Fakulti Sains Gunaan, Universiti Teknologi MARA Cawangan Perlis, MALAYSIA. E-mail: anglee631@uitm.edu.my[5]

[C]Lee Kong Chian Faculty of Engineering and Science, Universiti Tunku Abdul Rahman, 43200 Kajang, MALAYSIA. E-mail: simcl@utar.edu.my[6]

*Corresponding Author: tohpl@utar.edu.my

potential for future applications in the cosmetic industry, particularly in sunscreen products.

Among other initial studies, density functional theory (DFT) is one of the most widely used computational methods in recent years. Numerous DFT studies have been conducted to explore the electronic structures of BN systems (Roohi et al., 2010; Esrafili & Behzadi, 2012; Seyed–Talebi & Neek–Amal, 2014; Denis & Iribarne, 2019; Shuaibu et al., 2019; Toh & Wang, 2019). For example, Roohi et al. (2010) reported on the geometric structures and electronic properties of CH3CO molecules absorbed on the various surface sites of boron nitride nanotubes (BNNTs) at B3LYP/6–31G* level of theory. The DFT calculations indicated a preference for CH3CO molecules to absorb perpendicularly on the outer surfaces of BNNTs. In 2012, Esrafili and Behzadi presented the structural and electronic properties of carbon-doped BNNT using DFT/B3LYP/6–31G* level of calculation. In the context of carbon–doped BNNT, the obtained HOMO–LUMO energies were smaller than those of pure BNNT framework. Similarly, in 2014, Seyed-Talebi and Neek-Amal studied the absorption of methane molecules on the surfaces of BN and graphene sheets using B3LYP/6–31G* calculation. Computational results suggested a higher likelihood for methane molecules to absorb onto the surface of the BN monolayer than graphene. Similar findings were reported by Denis and Iribarne (2019). They investigated the adsorption of aryl, benzynes, ethyne, ethane, and azomethine on the surfaces of graphene and BN nanosheets using DFT/M06–L/6–31G* level of theory. The results for binding energy (BE) revealed a greater propensity for aryl, benzynes, ethyne, ethane, and azomethine molecules to absorb onto the BN system's surface rather than that of graphene. In the same year, Shuaibu et al. reported the elastic properties and electronic structures of h-BN monolayers through computational DFT investigations implemented in the Quantum-ESPRESSO program package. The computed findings identified a narrow band from the band structure calculations for the single layer of h-BN.
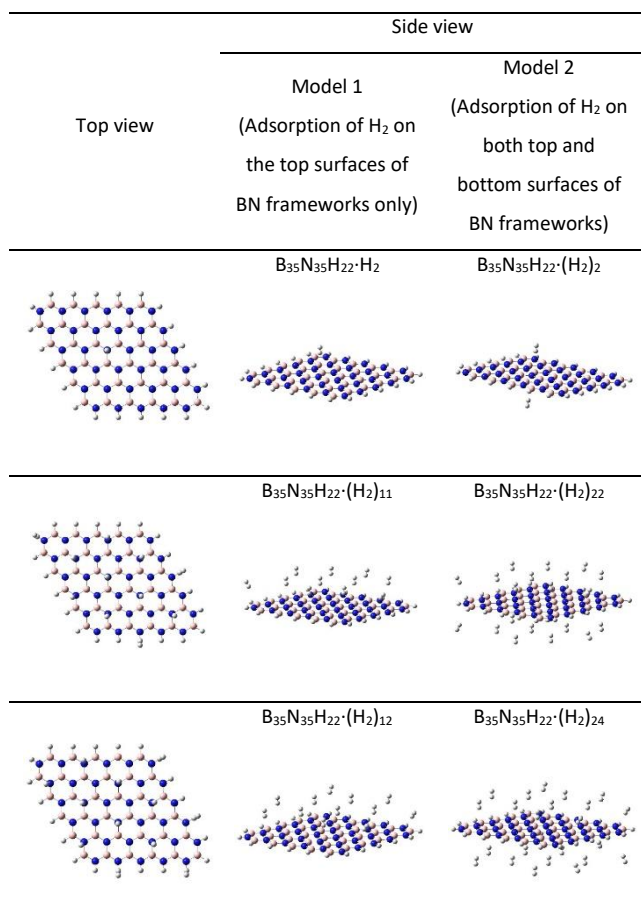
Furthermore, all elastic modulus constants, including shear strength and Young's modulus, strongly concur with the existing literature data. In 2019, Toh and Wang conducted computational studies on the structural and electronic structures of the h-BN nanosheet using the DFT technique, which was implemented within the Gaussian 09 software suite. They observed that the computed HOMO-LUMO energy gaps are about 6.0 eV - 7.7 eV, using B3LYP functional and four different basis sets. These energy values of HOMO-LUMO gaps were in excellent agreement with available experimental and computational data from prior studies (Oku, 2015; Lale et al., 2018; Chettri et al., 2021). In addition, Shah-Naqvi et al. (2022) also studied the structural and electronic properties of h-BN monolayers doped with or without group IV elements, i.e., carbon (C), silicon (Si), and germanium (Ge) atoms. The DFT results presented that the germanium-substituted BN system has the highest stability among all consideration BN frameworks.

In recent years, the literature on hydrogen storage materials has significantly increased in experimental and computational studies. This surge in research is attributed to hydrogen being a clean and renewable energy source. For example, using the DFT technique, Chettri et al. (2021) investigated the hydrogen storage capacity of monolayer h-BN nanosheets. The computed results indicated that the maximum hydrogen gravimetric density obtained in the studied h-BN nanosheet is about 6.7%, slightly higher than the Department of Energy (DOE) hydrogen storage targets of 6.0%. Therefore, numerous researchers have been interested in hydrogen as an energy source due to the growing role of hydrogen energy storage systems in future energy solutions, especially in transport, industry, cosmetics, and other sectors. From a literature survey, numerous studies have examined the technical and economic aspects of hydrogen energy systems (Oku, 2015; Lale et al., 2018). In 2015, Oku synthesized BN nanotubes, nano capsules, and nanocages and analysed their hydrogen storage capacity using thermogravimetric analysis (TGA). The experiment revealed that the BN nanostructures could only store hydrogen up to about 3 wt %.

Furthermore, semi-empirical molecular orbital calculations were conducted on the BN nanomaterials, yielding computed results that reported a hydrogen gravimetric capacity of approximately 6.5 wt%, in agreement with the DOE's target value. Lale et al. (2018) summarized BN nanostructures' potential for molecular hydrogen storage using the DFT technique, finding that among BN structures, the oxygen-doped BN nanosheet exhibits excellent material properties, providing the highest hydrogen storage capacity (about 5.8 wt%) in the literature survey. In 2021, Shah–Naqvi et al. reported a computational DFT investigation of two molecular hydrogen molecules adsorbed on the surfaces of BN nanostructures doped with or without group IV elements. The calculated binding energies of all the studied structures in the work were approximately 0.01 eV − 0.05 eV per molecular hydrogen. Motivated by the recent experimental and theoretical progress, conducting a computational DFT investigation into the adsorption of varying numbers of molecular hydrogens ($_{H2}$) onto boron nitride (BN) nanosheets is of great interest in this study.

2.   Computational Methodology

Top view	Side view	
	Model 1 (Adsorption of H_2 on the top surfaces of BN frameworks only)	Model 2 (Adsorption of H_2 on both top and bottom surfaces of BN frameworks)
	$B_{35}N_{35}H_{22} \cdot H_2$	$B_{35}N_{35}H_{22} \cdot (H_2)_2$
	$B_{35}N_{35}H_{22} \cdot (H_2)_{11}$	$B_{35}N_{35}H_{22} \cdot (H_2)_{22}$
	$B_{35}N_{35}H_{22} \cdot (H_2)_{12}$	$B_{35}N_{35}H_{22} \cdot (H_2)_{24}$

Figure 1. Top and side views for the adsorption of molecular hydrogens on the surfaces of BN monolayers.

All first principle DFT–based calculations were conducted using the Gaussian 09 software program (Frisch et al., 2016). Initially, the BN nanomaterial was selected for the study. Due to the absence of periodic boundary conditions in the DFT calculations, hydrogen (H) atoms were added to saturate the dangling bonds of B and N atoms in the BN structure (Zheng et al., 2011). Consequently, the cluster model of boron nitride $B_{35}N_{35}H_{22}$ was chosen as the local environment for this study. The molecular hydrogens (H_2) were also introduced to the surfaces of BN nanosheets. There are two H_2 adsorption configuration models employed in this study. Model 1 allows hydrogen molecules to adsorb solely on the BN sheets' top surfaces (one side). Conversely, model 2 assumes that the adsorption of molecular hydrogens on both surfaces (i.e., top and bottom sides) of BN monolayers. For both models (i.e., models 1 and 2), the H_2 molecules were sequentially added until the respective BN models reached their maximum H_2 capacity. Due to issues with self–consistent field convergence (SCF) in this work, geometry optimization calculations were employed to determine the

precise locations of H_2 molecules adsorption on the BN nanostructures at the DFT/B3LYP/6–31G level of theory.

Figure 1 illustrates three numbers of H_2 molecules (designated as 1, 11, and 12 in model 1) being adsorbed onto the top surfaces of BN frameworks. Additionally, three sets of molecular hydrogens (numbered 2, 22, and 24 in model 2) were placed on BN nanostructures' top and bottom surfaces. Single–point calculations were performed at the B3LYP/6–31G* level of theory to achieve more accurate energy levels. The equilibrium geometric structures resulting from the adsorption of H_2 molecules onto the studied BN systems were subsequently utilized to determine binding energies and various other electronic properties, including Frontier molecular orbitals (FMOs), molecular electrostatic potentials (MEPs), and others.

3.   Results and Discussions

In this study, the DFT technique is utilized to investigate the adsorption of hydrogen molecules on BN surfaces. Analysing the equilibrium structures of H_2 molecules adsorbed onto BN, as depicted in Figure 1, the computational results reveal optimized B–N bond lengths ranging from approximately 1.42 Å – 1.46 Å. These bond distances of BN closely align with experimental and previous theoretical findings (Anota et al., 2013; Thomas et al., 2020). Moreover, the results of the DFT calculations demonstrate a preference for hydrogen molecule adsorption on top of the nitrogen atoms. The molecular hydrogens are adsorbed to the surfaces of BN structures, with corresponding equilibrium distance ranging from 3.23 Å to 3.26 Å. The calculated H–H bond distances for hydrogen molecules in this study average around 0.74 Å.

Table 1 presents the binding energies of six numbers of H2 (i.e., 1, 2, 11, 12, 22, and 24) adsorbed onto the surfaces of BN monolayers, yielding values around about 0.01 eV. In addition, the DFT results reveal that the computed binding energies of BN frameworks are found depending on the quantity of adsorbed molecular hydrogen. In model 1, the binding energies follow this sequence: $B_{35}N_{35}H_{22} \cdot H_2$ > $BN_{35}H_{22} \cdot (H_2)11$ > $BN_{35}H_{22} \cdot (H_2)12$. Similarly, in model 2, the order is as follows: $B_{35}N_{35}H_{22} \cdot (H_2)_2$ > $B_{35}N_{35}H_{22} \cdot (H_2)_{22}$ > $B_{35}N_{35}H_{22} \cdot (H_2)_{24}$. Nevertheless, the computed binding energy values remain notably lower than the literature data (Chettri et al., 2021).

Table 1. Optimized hydrogen binding, BSSE, and Frontier molecular orbital energies (in eV) of BN nanostructures with the six numbers of molecular hydrogens.

Numbers of hydrogen molecules	Model 1			Model 2		
	$B_{35}N_{35}H_{22}{\cdot}H_2$	$B_{35}N_{35}H_{22}{\cdot}(H_2)_{11}$	$B_{35}N_{35}H_{22}{\cdot}(H_2)_{12}$	$B_{35}N_{35}H_{22}{\cdot}(H_2)_2$	$B_{35}N_{35}H_{22}{\cdot}(H_2)_{22}$	$B_{35}N_{35}H_{22}{\cdot}(H_2)_{24}$
Binding energy	0.0085	0.0077	0.0074	0.0085	0.0078	0.0074
BSSE	0.0135	0.1759	0.2011	0.0269	0.3476	0.3962
HOMO	−6.3147	−6.3544	−6.3781	−6.3158	−6.3917	−6.4325
LUMO	−0.3146	−0.3491	−0.3475	−0.3154	−0.3826	−0.3793
HOMO–LUMO energy	6.0001	6.0053	6.0306	6.0004	6.0091	6.0532

In Table 1, the HOMO–LUMO energies are determined to range between 6.00 eV – 6.05 eV. In the case of model 1, the HOMO–LUMO energy values exhibit an increase in the order as follows: $B_{35}N_{35}H_{22}{\cdot}H_2$ < $B_{35}N_{35}H_{22}{\cdot}(H_2)_{11}$ < $B_{35}N_{35}H_{22}{\cdot}(H_2)_{12}$. A similar pattern is observed in model 2, where the energy gap of HOMO–LUMO follows this progression: $B_{35}N_{35}H_{22}{\cdot}(H_2)_2$ < $B_{35}N_{35}H_{22}{\cdot}(H_2)_{22}$ < $B_{35}N_{35}H_{22}{\cdot}(H_2)_{24}$. Overall, as the number of molecular hydrogens in the investigated BN systems increases, there is a minimal alteration in the HOMO–LUMO energy values. The minimal alteration is attributed to the relatively modest interaction between the 1s–orbital of H and $2p_z$–orbitals of B and N atoms within the studied systems (Thomas et al., 2020).
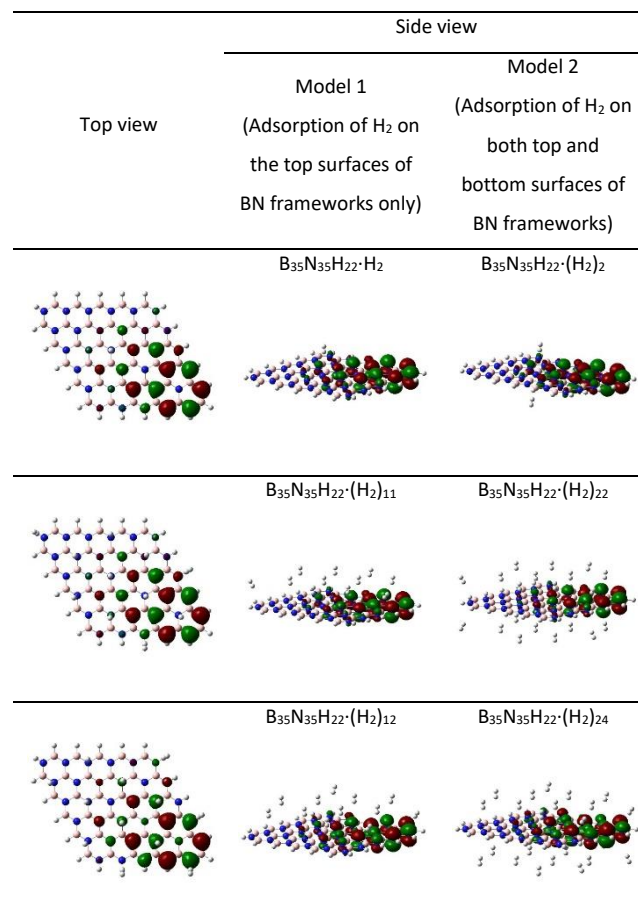
Figure 2. The diagrams of HOMO molecular orbitals for the various numbers of H_2 molecules absorbed on the surfaces of BN models.
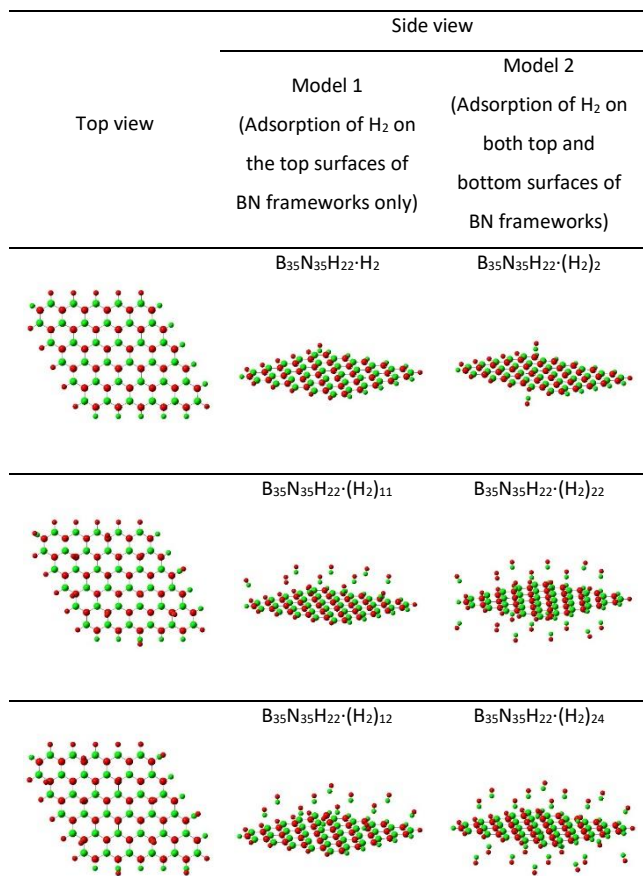
| Top view | Side view | |
	Model 1 (Adsorption of H_2 on the top surfaces of BN frameworks only)	Model 2 (Adsorption of H_2 on both top and bottom surfaces of BN frameworks)
	$B_{35}N_{35}H_{22} \cdot H_2$	$B_{35}N_{35}H_{22} \cdot (H_2)_2$
	$B_{35}N_{35}H_{22} \cdot (H_2)_{11}$	$B_{35}N_{35}H_{22} \cdot (H_2)_{22}$
	$B_{35}N_{35}H_{22} \cdot (H_2)_{12}$	$B_{35}N_{35}H_{22} \cdot (H_2)_{24}$
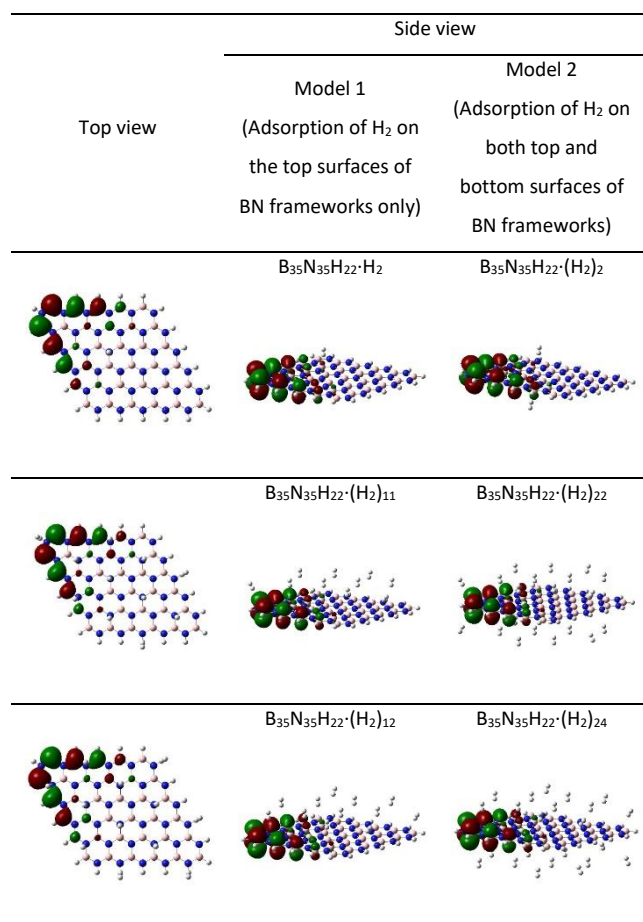
Figure 3. The molecular orbital diagrams of LUMOs for the adsorption of H_2 molecules on the surfaces of BN monolayers.

Thus, these HOMO–LUMO gap values closely resemble the bandgap obtained from previous literature studies (Toh & Wang, 2019; Chettri et al., 2021). To understand the adsorption interaction between molecular hydrogens and BN frameworks, the surface diagrams of the Frontier molecular orbitals of H_2 molecules adsorbed onto BN nanostructures are depicted in Figures 2 and 3. Our findings indicate that the distributions of Frontier molecular orbitals exhibit nearly identical patterns across all examined BN models (i.e., $B_{35}N_{35}H_{22} \cdot H_2$, $B_{35}N_{35}H_{22} \cdot (H_2)_2$, $B_{35}N_{35}H_{22} \cdot (H_2)_{11}$, $B_{35}N_{35}H_{22} \cdot (H_2)_{12}$, $B_{35}N_{35}H_{22} \cdot (H_2)_{22}$, and $B_{35}N_{35}H_{22} \cdot (H_2)_{24}$). The electron densities of HOMO orbitals, as shown in Figure 2, are localized in the N–edges of the studied BN systems. Conversely, 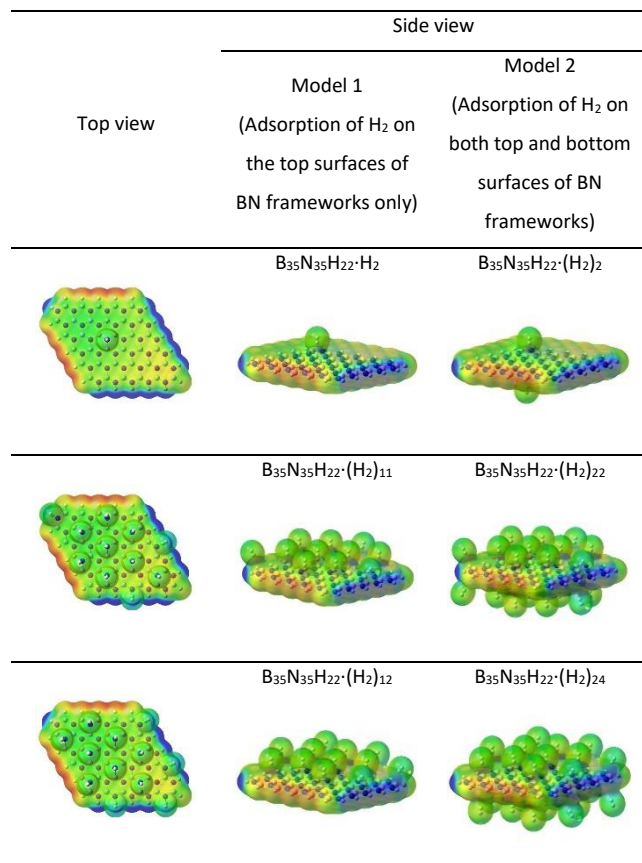for the LUMO orbitals illustrated in Figure 3, the electron density distribution predominantly centers around the B-edges. The HOMO predominantly exhibits p–character, originating from the p_z–orbitals of nitrogen atoms, while the LUMO primarily comprises p_z–orbitals from boron atoms at the edges. The results align with the findings presented by Javan et al. (2017). However, our findings explicitly indicate that an increase in the number of molecular hydrogens results in a minor but significant interaction between the 1s–orbital of H and $2p_z$–orbitals of B and N atoms within the studied BN systems (Anota et al., 2013).

Based on the Mulliken population analysis (MPA) shown in Figure 4, it is evident that the calculated results distribute negative charges (ranging from -0.626 a.u. and -0.434 a.u.) onto the nitrogen atoms within the BN frameworks. In contrast, the boron atoms exhibit notable high positive charges (falling within the range of +0.282 a.u. to +0.500 a.u.). In addition, the Mulliken scheme attributes both the positive and negative charge values to the hydrogen atoms, which depends on their localized bonding environment within the studied frameworks. Notably, the hydrogen atoms positioned at N-edges carry stronger positive charges (approximately +0.3 a.u.) than those at B-edges, which hold negative charges (approximately –0.05). It is also important to mention that neutral hydrogen molecules are obtained in this study. The distributions of MEPs for BN nanosheets hosting multiple hydrogen molecules are illustrated in Figure 5 to clarify the rationale behind this improvement. The MEP diagrams exhibit nearly identical map surfaces. This similarity stems from the minimal charge transfer from the BN framework to molecular hydrogens.

Additionally, the computed results indicate that the most positive electrostatic resides near nitrogen atoms, while the negative electrostatic potential is localized near B–edges. These computed findings align with the literature study conducted by Esrafili and Behzadi (2013). With these observations, the results obtained in this study hold great promise in guiding future investigations into single–wall or multi-wall boron nitride nanotube (BNNT) systems.

Top view	Side view	
	Model 1 (Adsorption of H_2 on the top surfaces of BN frameworks only)	Model 2 (Adsorption of H_2 on both top and bottom surfaces of BN frameworks)
	$B_{35}N_{35}H_{22} \cdot H_2$	$B_{35}N_{35}H_{22} \cdot (H_2)_2$
	$B_{35}N_{35}H_{22} \cdot (H_2)_{11}$	$B_{35}N_{35}H_{22} \cdot (H_2)_{22}$
	$B_{35}N_{35}H_{22} \cdot (H_2)_{12}$	$B_{35}N_{35}H_{22} \cdot (H_2)_{24}$

Figure 4. The distributions of Mulliken atomic charges for the various numbers of molecular hydrogens adsorbed on the surfaces of BN sheets.

Top view	Side view	
	Model 1 (Adsorption of H_2 on the top surfaces of BN frameworks only)	Model 2 (Adsorption of H_2 on both top and bottom surfaces of BN frameworks)
	$B_{35}N_{35}H_{22} \cdot H_2$	$B_{35}N_{35}H_{22} \cdot (H_2)_2$
	$B_{35}N_{35}H_{22} \cdot (H_2)_{11}$	$B_{35}N_{35}H_{22} \cdot (H_2)_{22}$
	$B_{35}N_{35}H_{22} \cdot (H_2)_{12}$	$B_{35}N_{35}H_{22} \cdot (H_2)_{24}$

Figure 5. Computed molecular electrostatic potential surface plots for the adsorption of molecular hydrogens on the surfaces of BN nanostructures.

4. Conclusion

This study reports the investigation of BN monolayers as potential H_2 molecular storage through DFT calculations. The molecular hydrogens exhibited favourable adsorption on the top of nitrogen atoms in BN nanosheets. The study performed DFT calculations to comprehend the binding energies and electronic structures of the BN models. The findings indicated that the computed binding energies obtained are approximately 0.01 eV per H_2 molecule. Moreover, the calculated results demonstrate that, for models 1 and 2, the binding energy increases proportionally with the number of molecular hydrogens adsorbed on the BN model's surface. A similar trend is evident in the case of the HOMO-LUMO energy value. The DFT results indicate that increasing the number of molecular hydrogens adsorbed onto the BN framework's surface significantly enhances the HOMO-LUMO gap value, which is approximately 6.0 eV for this study. Surface plots of HOMO and LUMO energies depict the calculated electron densities predominantly concentrated on the N- and B-edges, respectively.

In addition, this study explores the chemical reactivity of the investigated system investigated in this work. Positive and negative electrostatic potentials were identified within the systems. Notably, the most positive region was localized at the N-edge of the studied system, while the hydrogen atoms situated at the B-edge exhibited negative electrostatic potential. The distribution of Mulliken atomic charges illustrates positive charges for boron atoms in the BN models and negative charges for nitrogen atoms. Although the current models fall short of adsorbing molecular hydrogens effectively, the researchers believe that the computational findings lay the groundwork for future development of hydrogen storage materials in the future. Furthermore, it is suggested that Group IV-doped BN can be considered promising research for hydrogen storage study in future investigations.

5. Acknowledgement

6. References

Anota E. C., Juarez A. R., Castro M. & Cocoletzi H. H. (2013). A density functional theory analysis for the adsorption of the amine group on graphene and boron nitride nanosheets, *Journal of Molecular Modeling* 19: 321–328.

Ansaloni L. M. S. & Sousa E. M. B. d. (2013). Boron nitride nanostructures: Synthesis, characterization and potential use in cosmetics, *Materials Sciences, and Applications* 4: 22–28.

Chettri B., Patra P. K., Hieu N. N. & Rai D. P. (2021). Hexagonal boron nitride (h–BN) nanosheet as a potential hydrogen adsorption material: A density functional theory (DFT) study, *Surface and Interfaces* 24: 101043(1–8).

Denis P. A. & Iribarne F. (2019). Comparative study of the chemical reactivity of graphene and boron nitride sheets, *Computational and Theoretical Chemistry* 1164: 112538(1–7).

Esrafili M. D. & Behzadi H. (2012). A DFT study on carbon–doping at different sites of (8,0) boron nitride nanotube, Structural Chemistry 24(2): 573–581.

Esrafili M. D. & Behzadi H. (2013). A comparative study on carbon, boron–nitride, boron–phosphide, and silicon–carbide nanotubes based on surface electrostatic potentials and average local ionization energies, *Journal of Materials Chemistry A* 19(6): 2375–2382.

Frisch, M. J., Trucks, G. W., Schlegel, H. B., Scuseria, G. E., Robb, M. A., Cheeseman, J. R., Scalmani, G., Barone, V., Petersson, G. A., Nakatsuji, H., Li, X., Caricato, M., Marenich, A. V., Bloino, J., Janesko, B. G., Gomperts, R., Mennucci, B., Hratchian, H. P., Ortiz, J. V., Izmaylov, A. F., Sonnenberg, J. L., Williams–Young, D., Ding, F., Lipparini, F., Egidi, F., Goings, J., Peng, B., Petrone, A., Henderson, T., Ranasinghe, D., Zakrzewski, V. G., Gao, J., Rega, N., Zheng, G., Liang, W., Hada, M., Ehara, M., Toyota, K., Fukuda, R., Hasegawa, J., Ishida, M., Nakajima, T., Honda, Y., Kitao, O., Nakai, H., Vreven, T., Throssell, K., Montgomery, J. A., Jr., Peralta, J. E., Ogliaro, F., Bearpark, M. J., Heyd, J. J., Brothers, E. N., Kudin, K. N., Staroverov, V. N., Keith, T. A., Kobayashi, R., Normand, J., Raghavachari, K., Rendell, A. P., Burant, J. C., Iyengar, S. S., Tomasi, J., Cossi, M., Millam, J. M., Klene, M., Adamo, C., Cammi, R., Ochterski, J. W., Martin, R. L., Morokuma, K., Farkas, O., Foresman, J. B. & Fox, D. J., Gaussian 09, Wallingford CT, United Sate: Gaussian, Inc.

Gonzalez–Ortiz D., Salameh C., Bechelany M. & Miele P. (2020). Nanostructured boron nitride–based materials: synthesis and applications, *Materials Today Advances* 8: 100107(1–20).

Izyumskaya N., Demchenko D. O., Das S., Ozgur U., Avrution V. & Morkoc H. (2017). Recent development of boron nitride towards electronic applications, *Advanced Electronic Materials* 1600485(1–22).

Javan M. B., Soltani A., Ghasemi A. S., Lemeski E. T., Ghilami N., Balakheyli H. (2017). Ga–doped and antisite double defects enhance the sensitivity of boron nitride nanotubes towards soman and chlorosoman, *Applied Surface Science* 411: 1–10.

Kannan P. K., Saraswathi R. & Bercamans L. J. (2013). Combustion synthesis of boron nitride by glycine route, *Research Journal of Chemical Sciences* 3(2): 59–64.

Lale A., Bernard S. & Demirci U. B. (2018). Boron nitride for hydrogen storage, *ChemPlusChem* 83(10): 893–903.

Mukasyan A. S. (2017). Boron Nitride, Concise Encyclopedia of Self–Propagating High–Temperature Synthesis, pp. 45–47, Amsterdam, Netherlands: Elsevier.

Oku, T. (2015). Hydrogen storage in boron nitride and carbon nanomaterials, *Energies* 8(1): 319–337.

Roohi H., Nowroozi A., Ebrahimi A. & Makiabadi B. (2010). Effect of CH_3CO functional group on the molecular and electronic properties of BN43zz nanotube: A computational chemistry study, *Journal of Molecular Structure: THEOCHEM* 952: 36–45.

Seyed–Talebi S. M. & Neek–Amal M. (2014). The different adsorption mechanism of methane molecule onto a boron nitride and a graphene flakes, *Journal of Applied Physics* 116(15): 153507(1–7).

Shah–Naqvi S. A. A., Toh P. L., Lim Y. C., Wang S. M., Ang L. S. & Sim L. C. (2022). Computational density functional theory investigation of stability and electronic structures on boron nitride systems doped with/without group IV elements, *Malaysian Journal of Chemistry* 24(1): 85–93.

Shah–Naqvi S. A. A., Toh P. L., Lim Y. C., Wang S. M., Ang L. S. & Sim L. C. (2021). Computational study of hydrogen molecules adsorption on boron nitride with/without adopted by one of elements from group IV, *IOP Conference Series Earth and Environmental Science* 945(1): 012001(1–12).

Shuaibu A., Adeyemi O. J. & Usiekpan U. R. (2019). First principle study of structural, elastic and electronic properties of hexagonal boron nitride (Hex–BN) single layer, *American Journal of Condensed Matter Physics* 9(1): 1–5.

Thomas S., Manju M. S., Ajith K.M., Lee S.U., Zaeem M. A. (2020). Strain–induced work function in h–BN and BCN monolayers, *Physica E: Low–Dimensional Systems and Nanostructures* 123: 114180(1–9).

Toh P. L. & Wang S. M. (2019). Theoretical investigations of the structural and electronic properties of boron nitride clusters: DFT comparison of several basis sets, *Journal of Physics: Conference Series* 1349: 012137(1–6).

Zheng F. L., Zhang Y., Zhang J. M. & Xu K. W. (2011). Effect of the dangling bond on the electronic and magnetic properties of BN nanoribbon, *Journal of Physics and Chemistry of Solids* 72(4): 256–262.